BIOCHEMISTRY
including biophysical chemistry & molecular biology

Article

pubs.acs.org/biochemistry

Characterization of Heme Ligation Properties of Rv0203, a Secreted Heme Binding Protein Involved in *Mycobacterium tuberculosis* Heme Uptake

Cedric P. Owens,[†] Jing Du,[§] John H. Dawson,[§,∥] and Celia W. Goulding*[,†,‡]

[†]Department of Molecular Biology and Biochemistry and [‡]Department of Pharmaceutical Sciences, University of California, Irvine, California 92697, United States

[§]Department of Chemistry and Biochemistry and [∥]School of Medicine, University of South Carolina, Columbia, South Carolina 20208, United States

Supporting Information

ABSTRACT: The secreted *Mycobacterium tuberculosis* (Mtb) heme binding protein Rv0203 has been shown to play a role in Mtb heme uptake. In this work, we use spectroscopic (absorption, electron paramagnetic resonance, and magnetic circular dichrosim) methods to further characterize the heme coordination environments of His-tagged and native protein forms, Rv0203-His and Rv0203-notag, respectively. Rv0203-His binds the heme molecule through bis-His coordination and is low-spin in both ferric and ferrous oxidation states. Rv0203-notag is high-spin in both oxidation states and shares spectroscopic similarity with pentacoordinate oxygen-ligated heme proteins. Mutagenesis experiments determined that residues Tyr59, His63, and His89 are required for Rv0203-notag to efficiently bind heme, reinforcing the hypothesis based on our previous structural and mutagenesis studies of Rv0203-His. While Tyr59, His63, and His89 are required for the binding of heme to Rv0203-notag, comparison of the absorption spectra of the Rv0203-notag mutants suggests the heme ligand may be the hydroxyl group of Tyr59, although an exogenous hydroxide cannot be ruled out. Additionally, we measured the heme affinities of Rv0203-His and Rv0203-notag using stopped flow techniques. The rates for binding of heme to Rv0203-His and Rv0203-notag are similar, 115 and 133 μM^{-1} s^{-1}, respectively. However, the heme off rates differ quite dramatically, whereby Rv0203-His gives biphasic dissociation kinetics with fast and slow rates of 0.0019 and 0.0002 s^{-1}, respectively, and Rv0203-notag has a single off rate of 0.082 s^{-1}. The spectral and heme binding affinity differences between Rv0203-His and Rv0203-notag suggest that the His tag interferes with heme binding. Furthermore, these results imply that the His tag has the ability to stabilize heme binding as well as alter heme ligand coordination of Rv0203 by providing an unnatural histidine ligand. Moreover, the heme affinity of Rv0203-notag is comparable to that of other heme transport proteins, implying that Rv0203 may act as an extracellular heme transporter.

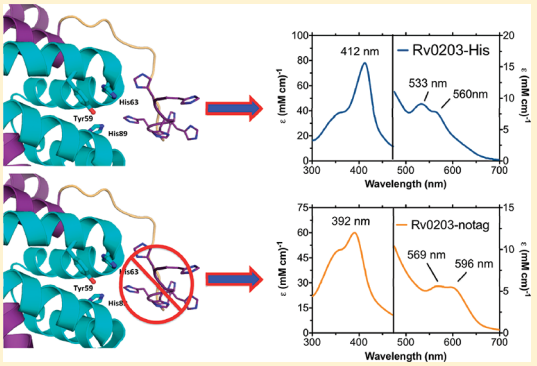

Mycobacterium tuberculosis (Mtb) is the causative agent of tuberculosis (TB), a disease responsible for approximately 1.5 million deaths per year.[1] During its infection, Mtb has to maintain iron homeostasis while residing in its human host. Mtb has therefore developed a sophisticated siderophore-mediated iron uptake pathway, which can scavenge non-heme iron from a variety of sources, including the human iron transport protein transferrin, and subsequently transfers scavenged iron to membrane-bound mycobactin[2−4] or the iron transport system, IrtA/B.[5] This pathway, however, is metabolically costly because mycobactin biosynthesis requires at least 11 different enzymes.[6] Moreover, the human innate immune system features a siderophore binding protein, siderocalin, which sequesters siderophores and has been shown to inhibit Mtb replication in macrophages by disrupting the bacterium's siderophore-mediated iron scavenging abilities.[7]

An alternative form of iron uptake is via the ubiquitous heme group that contains iron. Over the last two decades, heme acquisition pathways have been discovered in a growing number of bacteria. The ability to acquire heme has been demonstrated to enhance bacterial virulence in two species, *Staphylococcus aureus*[8] and *Escherichia coli*.[9] There are several mechanisms of heme acquisition; the ligand can be acquired by cell surface-associated heme and hemoprotein receptors,[10−13] by secreted high-affinity heme scavengers (hemophores),[14−17] and in conjunction with hemoprotein-specific proteases.[18−20] Recently, studies have shown that mycobacteria may utilize heme as an alternative iron source.[21−23] Experiments using a siderophore knockout of Mtb (MtbΔ*mbtB*) showed that heme can sustain bacterial growth in vitro,[22] whereas it was observed that the attenuated *Mycobacterium bovis* strain, Bacille Calmette-Guérin siderophore knockout mutant (BCGΔ*mbtB*), grew

Received: July 11, 2011
Published: January 23, 2012

   dx.doi.org/10.1021/bi2018305 | *Biochemistry* 2012, 51, 1518−1531

in a mouse model, suggesting that this mutant utilized heme as an iron source in vivo.[21] A region of the Mtb genome encoding seven mycobacterium-specific proteins (Rv0201c−Rv0207c) has been identified as being essential for Mtb heme uptake.[22] A secreted protein, Rv0203, is encoded in this genomic region. Rv0203 has a low degree of sequence homology with all other nonmycobacterial proteins in the NCBI database and no assigned function until this point. The role of Rv0203 in heme uptake was investigated by double-knockout experiments (MtbΔ*mbtB*Δ*Rv0203*), which demonstrated that Rv0203 is required for efficient growth of MtbΔ*mbtB* in heme-containing media, although Rv0203 is not essential for survival under these in vitro conditions.[22] Furthermore, Rv0203 is the only Mtb culture filtrate (secreted) protein that binds to heme-agarose, and it has been shown that the mature, His-tagged form of recombinant Rv0203 (Rv0203-His with no signal peptide) binds heme.[22]

The apo crystal structure of Rv0203-His has been determined. It is entirely α-helical and features a novel fold.[22] Analysis of the apo-Rv0203-His structure revealed a heme binding motif similar to that of *Serratia marcescens* HasA[24] (a well-characterized hemophore) whereby His89 is 7.8 Å from Tyr59, which is hydrogen-bonded to His63 (Figure 1), leading

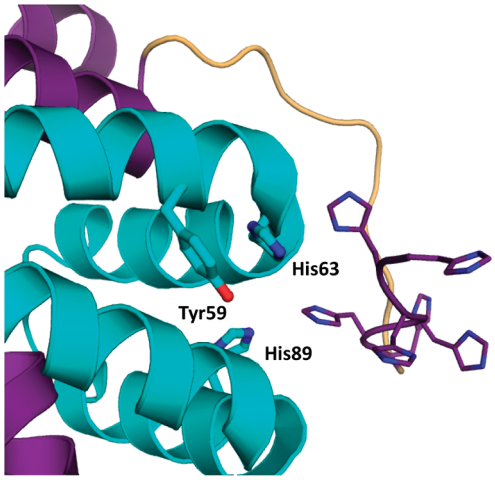

Figure 1. Crystal structure of apo-Rv0203 (PDB entry 3MAY), including a manually built-in N-terminal His tag. Residues MHHHHHHGSVPRGAS were not observed in the electon density map of Rv0203 and were built using COOT[61] solely to illustrate how the His tag may come into the proximity of the proposed heme binding site. Polypeptide chains A and B are in represented as cartoons and colored purple and cyan, respectively. The proposed active site residues, Tyr59, His63, and His89, are shown as sticks, and the His residues from the His tag are represented as lines.

to the hypothesis that Tyr59, His63, and His89 may represent the Rv0203 heme binding site. This hypothesis was reinforced through the observation that the Y59A-Rv0203-His mutant does not bind heme, although both the H63A- and H89A-Rv0203-His mutants retain heme binding properties similar to those of WT-Rv0203-His.[22]

In this work, we have produced a tagless version of Rv0203 (Rv0203-notag) and provide evidence that the His tag of Rv0203-His interferes with heme binding and acts as an unnatural ligand to the heme iron. While Rv0203-notag retains the ability to bind heme, it displays differences in both heme coordination and heme binding affinity compared to those of Rv0203-His. Mutational analysis indicates that the heme binding site of Rv0203-notag consists of Tyr59, His63, and His89, which are the same residues identified for Rv0203-His.[22] However, the UV−visible (UV−vis) absorption and magnetic circular dichroism (MCD) spectra indicate the coordination structure of the heme iron in Rv0203-His is bis-His, whereas Rv0203-notag binds heme through an oxygen ligand. The heme binding affinities of both Rv0203-His and Rv0203-notag were measured using stopped flow techniques, which showed that the affinity of Rv0203-notag for heme is approximately 2 orders of magnitude lower than that of Rv0203-His. The heme binding affinity of Rv0203-notag is similar to that of several heme-trafficking proteins but lower than that of the well-characterized hemophore HasA,[25] suggesting that Rv0203 does not scavenge heme by an affinity-driven mechanism.

MATERIALS AND METHODS

Cloning, Expression, and Purification of Rv0203. The cloning, expression, and purification protocols for Rv0203-His and Mtb proteins have been described previously.[26] Briefly, for Rv0203-notag, the truncated gene encoding mature Rv0203 (residues 36−136) was cloned into pET30a (Stratagene) using *Nco*I and *Hin*dIII restriction enzyme sites to produce a fusion protein with an N-terminal enterokinase-cleavable His tag. After enterokinase cleavage, three amino acid (AMA) residues represent the only non-native N-terminal residues of Rv0203-notag. For Rv0203-His (N-terminally His-tagged fusion protein), the truncated gene encoding residues 36−136 was cloned into pQE30 (Qiagen), as described previously.[22] The translated protein sequence contains 15 non-native amino acid residues at the N-terminus (MRGSHHHHHHGSVPR).

Plasmids expressing Rv0203-notag and Rv0203-His were transformed into BL21-Gold (DE3) and XL1 Blue cells, respectively. Cells were grown at 37 °C in LB medium containing 30 μg/mL kanamycin or 50 μg/mL ampicillin for Rv0203-notag or Rv0203-His, respectively. Protein expression was induced when cells reached an OD of approximately 0.8 by the addition of 1 mM isopropyl β-D-1-thiogalactopyranoside. The cells were harvested after 4 h by centrifugation at 5100 rpm for 20 min and resuspended in 50 mM Tris (pH 7.4) and 350 mM NaCl.

The cells were lysed by sonication after addition of egg hen lysozyme and phenylmethanesulfonyl fluoride. The cell lysate was centrifuged at 14000 rpm for 30 min and the supernatant collected. After addition of 400 μL of Proteoblock protease inhibitor cocktail (Fermentas), the supernatant was loaded onto a Ni^{2+}-charged HisTrap column (GE Healthcare) and eluted with a linear imidazole gradient. Both Rv0203 His-tagged constructs (Rv0203-notag prior to enterokinase treatment and Rv0203-His) eluted between 200 and 300 mM imidazole. Fractions containing Rv0203 His-tagged proteins were identified by SDS−PAGE, pooled, and concentrated using a Centricon centrifugal concentrator (Millipore). Final purification of Rv0203-His was achieved by running the protein over an S75 gel filtration column (GE Healthcare) equilibrated with 50 mM Tris (pH 7.4) and 150 mM NaCl, which yielded nearly 100% pure protein. To produce Rv0203-notag, Rv0203 with a cleavable His tag was further purified over an S75 gel filtration column and buffer exchanged into cleavage buffer [20 mM Tris (pH 7.4), 50 mM NaCl, and 2 mM $CaCl_2$]. Fractions containing the protein of interest were identified by SDS−PAGE, pooled, and diluted to approximately 1 mg/mL protein. Cleavage of the His tag was accomplished by adding 10 activity units of recombinant enterokinase (Novagen) to the

dx.doi.org/10.1021/bi2018305 | *Biochemistry* 2012, 51, 1518−1531

protein. The cleavage reaction was monitored by SDS−PAGE and run until it was complete. Recombinant enterokinase was removed using a Recombinant Enterokinase Capture Kit (Novagen). The cleaved His tag was separated from Rv0203-notag by adding NaCl to a concentration of 1 M and loading the protein onto a Ni^{2+}-charged HiTrap column (GE Healthcare). The flow-through and protein that eluted at 10 mM imidazole were collected. The final purification step of Rv0203-notag over an S75 gel filtration column yielded nearly 100% pure protein. All experiments were performed in 50 mM Tris (pH 7.4) and 150 mM NaCl unless otherwise stated.

Site-Directed Mutagenesis. The Y59A-, Y59H-, Y59F-, H63A-, and H89A-Rv0203-notag single mutants were created by in vitro site-directed mutagenesis using the Quick Change site-directed mutagenesis kit (Stratagene). The H63A/H89A-Rv0203-notag double mutant was produced by introducing the H63A mutation into the plasmid containing H89A-Rv0203-notag. The purification procedure for the mutant forms of Rv0203-notag is identical to that of the wild-type protein.

Preparation of the Heme Solution and Reconstitution of Apoproteins. Approximately 4 mg of heme was dissolved in 0.4 mL of ice-cold 0.1 M NaOH and vortexed periodically. After 30 min, 0.4 mL of 1 M Tris (pH 7.4) was added to the solution. The solution was subsequently centrifuged for 10 min at 4 °C and 13000 rpm. The supernatant was then diluted with 50 mM Tris (pH 7.4) and 150 mM NaCl and centrifuged again at 5100 rpm for 10 min to remove any heme aggregates. Final concentrations were determined using an ε_{385} of 58.44 mM^{-1} cm^{-1}.[27] Heme solutions were used within 12 h.

Apoprotein was reconstituted by slowly adding a 1.25-fold excess of heme to the apoprotein and subsequently nutating the protein at 4 °C overnight. Excess heme was removed from Rv0203-His and Rv0203-notag by passing the samples over a G-25 desalting column (GE Healthcare). The heme contents of the holoproteins were measured using the pyridine hemochromagen assay,[28] and the protein concentration was measured by the modified Lowry assay (Pierce).

To make unsaturated Rv0203-notag for the ferrous Rv0203-notag UV−vis absorption spectrum and for the off-rate experiment with unsaturated Rv0203-notag, apo-Rv0203-notag was reconstituted with heme:protein ratios of 1:10 and 1:3.3, respectively.

Ferrous hemoproteins were made by anaerobic reduction with sodium dithionite. Between 1 and 2 mM aqueous sodium dithionite was added to degassed ferric protein from a stock solution of 200 mM sodium dithionite, dissolved in 50 mM Tris (pH ∼9.0) and 150 mM NaCl. The ferrous CO adducts of Rv0203-notag and Rv0203-His were prepared by saturating the reduced holoprotein solutions with CO gas.

Spectroscopic Measurements. All absorption spectra were recorded at room temperature on a Beckman DU800 spectrophotometer using cells with a 1 cm path length, except for heme titration measurements, which were conducted on a Varian Cary 3E dual-beam spectrophotometer.

MCD spectra were measured with a magnetic field strength of 1.41 T by using a JASCO J815 spectropolarimeter. This instrument was equipped with a JASCO MCD-1B electromagnet and interfaced with a Silicon Solutions personal computer through a JASCO IF-815-2 interface unit. All spectral measurements were performed using a 0.2 or 1.0 cm cuvette at 4 °C. Data acquisition and manipulation have been described previously.[29] UV−visible absorption spectra were recorded before and after the MCD measurements to verify sample integrity.

Electron paramagnetic resonance (EPR) spectra were recorded on a Bruker EMX500 spectrometer fitted with a Bruker ER041x microwave bridge and an Oxford Instruments continuous flow liquid He cryostat. The temperature was maintained at 4.5 K and monitored using an Oxford ITC503S temperature control unit. The magnetic field frequency was calibrated using a 2,2-diphenyl-1-picrylhydrazyl (DPPH) standard (g = 2.0036).

Far-UV circular dichroism (CD) spectra were recorded at 4 °C on a Jasco J-715 spectropolarimeter using 0.1 cm path length cells. The bandwidth was set to 0.5 nm; the response time was 2 s, and the wavelength step was equal to 0.2 nm per increment.

Heme Titration. Small amounts of a concentrated heme solution (∼250 μM) in 50 mM Tris (pH 7.4) and 150 mM NaCl were titrated into cuvettes containing either protein or buffer. Spectra were recorded after a 5 min incubation period at room temperature.

Preparation of Apo-H64Y/V68F-Mb. A dilute solution (approximately 50 μM) of H64Y/V68F-Mb[30] was acidified to pH 3.0 on ice, and heme was extracted using two equal-volume washes of ice-cold methyl ethyl ketone. Apo-H64Y/V68F-Mb was then extensively dialyzed at 4 °C against 50 mM Tris (pH 7.4) and 150 mM NaCl to remove methyl ethyl ketone and the protein concentration measured using an ε_{280} of 17 mM^{-1} cm^{-1}.

Off-Rate Measurement (apomyoglobin assay). To measure heme dissociation, holo-Rv0203-notag and a 10-fold excess of H64Y/V68F-Mb were mixed in an SX.18MV stopped flow spectrophotometer (Applied Photophysics) by rapid, equal-volume mixing at room temperature. The reaction was monitored at 410 or 600 nm until it was complete. The rate of dissociation of heme from holo-Rv0203-His was measured in a conventional spectrophotometer by mixing the holoprotein with a 10-fold excess of apo-H64Y/V68F-Mb and monitoring the reaction at 600 nm for up to 3 h. The resulting time courses for both Rv0203-notag and Rv0203-His were fitted to single- and double-exponential functions using Graphpad Prism.

For the off-rate measurements of the various Rv0203-notag mutants, the holoprotein:apo-H64Y/V68F-Mb concentration ratio was 1:10 (protein:protein). Because it is not possible to fully heme load the mutant proteins, especially Y59A- and H63A/H89A-Rv0203-notag, the heme contents of each mutant are different. To permit visual comparison between mutants, the data were normalized between 0 and 100, such that 100 equals the respective total differential absorption over the course of the experiment for each mutant. As discussed in Results, the percentage of heme loading is not expected to affect the off rate as long as apo-H64Y/V68F-Mb is in excess.

On-Rate Measurement. Stocks of ferrous CO-heme were made by anaerobically reducing fresh heme solutions at various concentrations with 2 mM sodium dithionite and then bubbling CO through the ferrous heme solutions. The heme concentrations of the ferrous CO-heme stock were verified using an ε_{407} of 147 mM^{-1} cm^{-1}.[31] Holoprotein samples were degassed, reduced with 2 mM sodium dithionite, and saturated with CO.

Stopped flow measurements were taken in an anaerobic environment by equal-volume mixing in an Applied Photophysics SX.18MV device at room temperature. The loading syringes were assembled in an anaerobic glovebox and fitted to

the vertical position of a three-way stopcock. A wash syringe containing CO-saturated buffer and 2 mM dithionite was attached to the horizontal position of the stopcock and used to purge the stopped flow system before each experiment.

Initially, the reaction of either 2 μM apo-Rv0203-notag or apo-Rv0203-His with 1 μM ferrous CO-heme was measured by time-resolved rapid scan spectrophotometry to determine the wavelength of maximal absorbance change, which is 427 nm for both proteins. This method was also used to determine the values of k_{obs} for wild-type (WT) Rv0203-notag and the various mutants. On rates, k_{on}, for Rv0203-notag and Rv0203-His were determined by mixing various concentrations of apoprotein with 0.5 μM ferrous CO-heme and monitoring the reactions at 427 nm in photomultiplier mode. The experimental data were monophasic and fit to single-exponential curves using Graphpad Prism. At apoprotein concentrations of >3 μM, a large portion of the reaction occurs within the 2 ms dead time of the instrument. It should be noted that the values in the k_{obs} measurement differ from those in the on-rate experiment because of the different instrument settings, diode array mode and photomultiplier mode, respectively. Diode array mode records fewer data points in the first millisecond of the reaction and therefore produces a smaller value for k_{obs}.

RESULTS

Heme Reconstitution and Heme Titration of Rv0203. Recombinant Rv0203-His was expressed as a fusion protein with a noncleavable N-terminal His tag. A new construct was engineered to produce Rv0203 with an N-terminal enterokinase-cleavable His tag to produce Rv0203-notag. After enterokinase cleavage, three non-native amino acid residues remain on the N-terminus of Rv0203-notag (AMA). Both proteins are present as predominantly apoproteins with no endogenous heme content (<1%) after purification by Ni^{2+} affinity followed by gel filtration chromatography. Previously, it has been shown that Rv0203-His binds heme in a 1:1 heme:protein ratio.[22] A heme titration experiment with Rv0203-notag indicates that the binding stoichiometry is also 1:1 (Figure 2). To reconstitute the apoproteins, heme was

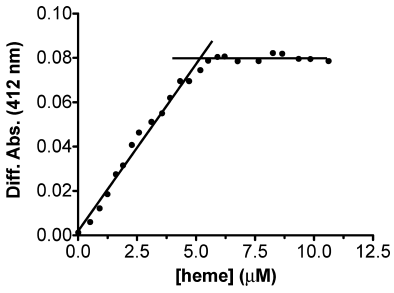

Figure 2. Heme titration experiments with 5 μM apo-Rv0203-notag indicating 1:1 heme:protein stoichiometry. The curve was generated by measuring the difference spectrum between the protein sample and heme-only sample to determine the wavelength of maximal absorbance difference, which was 412 nm. The saturation concentration is reached when the differential absorbance remains constant.

added to both Rv0203-His and Rv0203-notag to a 1.25-fold molar excess and unbound heme removed over a desalting column, which produces rust-colored holo-Rv0203-His and green-colored holo-Rv0203-notag.

The oxidation state of both reconstituted holoproteins was determined by adding the oxidizing agent potassium ferricyanide to the holoproteins and observing the change in the absorption spectrum between 450 and 700 nm, a region sensitive to the oxidation state of the iron. Addition of ferricyanide did not alter the absorption spectra of either Rv0203-notag or Rv0203-His, indicating that the aerobically reconstituted proteins are both present in their ferric states (Figure S1 of the Supporting Information).

Heme Binding Does Not Change the Secondary Structure or Oligomeric State of Rv0203-notag. To ensure that no large secondary structure changes occurred upon heme binding, the far-UV CD spectra of holo- and apo-Rv0203-notag were recorded, as shown in Figure 3. The spectra of holo-

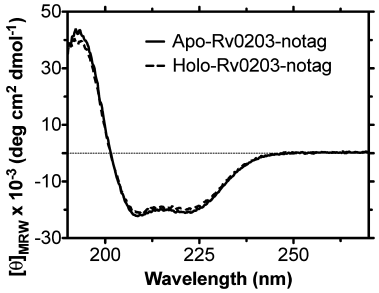

Figure 3. Far-UV CD spectrum of apo-Rv0203-notag compared with that of holo-Rv0203-notag. The protein concentration was 10.75 μM for apo-Rv0203-notag and 7.5 μM for holo-Rv0203-notag in 5 mM phosphate buffer (pH 7.4). Each spectrum represents the average of two scans.

and apo-Rv0203-notag are identical and predominantly α-helical, thus ruling out significant secondary structure perturbation upon heme binding. These results reflect what had previously been reported for Rv0203-His.[22] The oligomeric states of holo- and apo-Rv0203-notag were determined by analytical gel filtration chromatography, and both apo- and holo-Rv0203-notag elute as a dimer (Figure S2 of the Supporting Information).

Absorption and MCD Spectra of Holo-Rv0203-His. The absorption spectra of ferric and ferrous forms of holo-Rv0203-His and its ferrous carbonyl adduct are shown in Figure 4a. Ferric holo-Rv0203-His has a Soret peak at 412 nm and a visible maximum at 533 nm with a shoulder at 560 nm, indicating a low-spin ($S = {}^1/_2$), six-coordinate ferric complex, which has spectral features similar to those of as hexacoordinate bis-His-ligated heme proteins (Table 1). The ferric absorption spectrum also has a small feature at 350 nm, indicative of a minor amount of high-spin heme. Upon anaerobic reduction of holo-Rv0203-His with sodium dithionite, a red shift in the Soret peak to 426 nm is apparent, as is the emergence of two distinct peaks at 530 and 559 nm (Figure 4a), which indicates that the heme iron retains its low-spin six-coordinate structure in the ferrous state (Figure 4a). Inspection of ferric and ferrous Rv0203-His MCD (Figure 5a) spectra reveal similarities with bis-His heme-coordinated proteins, including cytochrome b_5 (Table 2) and H93G-Mb (bis-imidizole),[40] indicating that the most likely coordination mode for holo-Rv0203-His is bis-His.

Absorption and MCD Spectra of Holo-Rv0203-notag. The UV−vis absorption spectrum of ferric holo-Rv0203-notag is shown in Figure 4b and features a relatively weak and broad Soret peak with a maximum at 392 nm and two broad visible peaks around 569 and 596 nm. The location of the Soret peak below 400 nm and the charge transfer band at 596 nm indicate the heme iron is high-spin ($S = {}^5/_2$). Investigation of the

dx.doi.org/10.1021/bi2018305 | Biochemistry 2012, 51, 1518−1531

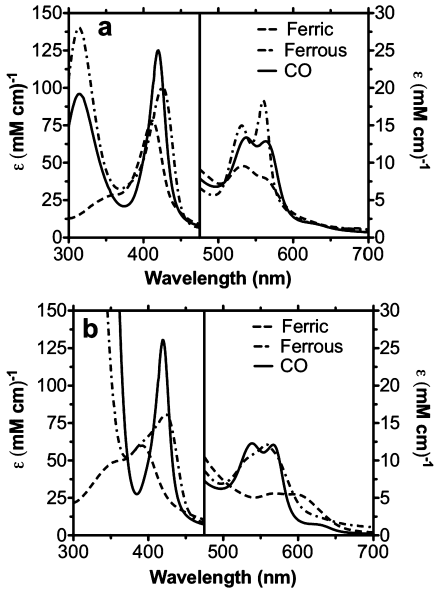

Figure 4. UV−vis absorption spectra of (a) holo-Rv0203-His and (b) holo-Rv0203-notag in 50 mM Tris (pH 7.4) and 150 mM NaCl. The ferric holoproteins are prepared as described in Materials and Methods. The ferrous derivatives were produced by anaerobically adding 1 mM sodium dithionite to either ferric holo-Rv0203-notag or holo-Rv0203-His. The ferrous CO adducts were produced by bubbling CO gas through the ferrous holoproteins. The extinction coefficients of the holoproteins are based on the heme contents.

Table 1. Comparison of the Absorption Features of Ferric Holo-Rv0203-notag and Holo-Rv0203-His with Five- and Six-Coordinate Heme Complexes from the Literature[a]

protein (ref)	ligands	Soret (nm) [ε (mM^{-1} cm^{-1})]	visible (nm)
Rv0203-His (this work)	His, His	412 (78)	533, 560
Rv0203-notag (this work)	O	392 (60)	569, 596
cytochrome b_5[32]	His, His	412 (116)	531, 559
neuroglobin[33]	His, His	413	533, 562
HasA[34]	His, Tyr	406	494, 537, 568, 618
H25Y-hHO-1[35]	Tyr	393	500*, 612
Dap1p[36]	Tyr	398	500, 530, 620
H93Y-swMb[37]	Tyr	402 (100)	480, 524, 598
H93G-Mb (alkaline)[38]	OH^-	403 (104)	482, 600
H93G-Mb (BME)[39]	S^-	391 (65*)	510, 618
heme (pH 7.4)	OH^-	385 (58)	611

[a]Extinction coefficients and peaks marked with asterisks were estimated by visual inspection.

literature did not reveal a known high-spin heme protein that was greatly spectrally similar with Rv0203-notag, which suggests Rv0203-notag has a unique heme coordination environment (Table 1). The closest spectroscopic resemblance is found between ferric holo-Rv0203-notag and pentacoordinate heme proteins with anionic ligands, which are known to feature a relatively weak Soret peak at wavelengths below 400 nm and a charge transfer band near 600 nm.

Reduction of holo-Rv0203-notag by sodium dithionite produces a red-shifted Soret peak and merged α- and β-bands. However, the Soret peak is broad and resembles that of

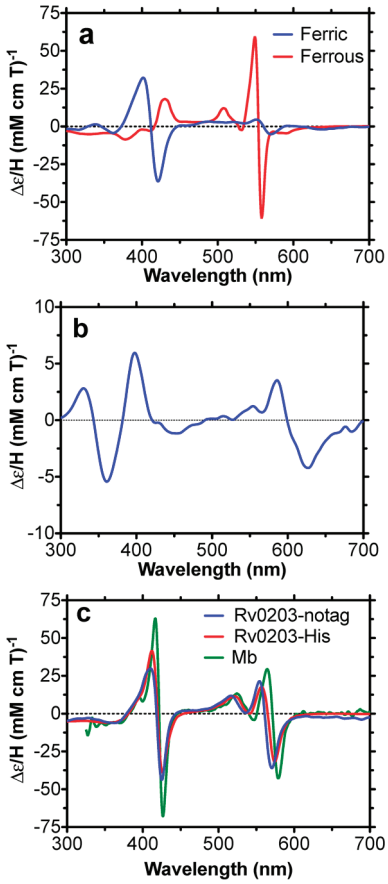

Figure 5. MCD spectra of (a) ferric and ferrous holo-Rv0203-His, (b) ferric holo-Rv0203-notag, and (c) the ferrous CO adducts of holo-Rv0203-notag and holo-Rv0203-His in 50 mM Tris (pH 7.4) and 150 mM NaCl compared to that of myoglobin (Mb) in 100 mM potassium phosphate buffer (pH 7) at 4 °C.

partially acid denatured deoxymyoglobin,[41] indicating that heme has partially dissociated from holo-Rv0203-notag (Figure S3 of the Supporting Information). To characterize heme-bound ferrous Rv0203-notag, an unsaturated form of holo-Rv0203-notag was produced that was more refractory to heme loss, whereby the heme:protein ratio in the sample is 1:10. After reduction of unsaturated holo-Rv0203-notag, the Soret peak maximum shifts to 423 nm, and a single peak emerges at 557 nm (Figure 4b), indicating a high-spin five-coordinate heme iron structure. The observation that excess Rv0203-notag is required to bind ferrous heme suggests that Rv0203-notag binds heme less tightly in the ferrous oxidation state than in the ferric state.

Further characterization of ferric holo-Rv0203-notag was undertaken using MCD spectroscopy. The overall MCD intensity of ferric holo-Rv0203-notag is relatively weak. In particular, the location of the absorbance maximum at 398 nm and two minima at 527 and 627 nm and the spectral shape in the visible region (Figure 5b) share some commonality with the MCD spectra of five-coordinate oxygen-bound heme molecules such as the myoglobin cavity mutant H93Y-Mb that has a tyrosine ligand,[38] and methoxide-ligated Fe-protoporphyrin IX dimethyl ester (Fe-PPIXDME)[38] (Table 3).

Ferrous Carbonyl Adducts of Holo-Rv0203-notag and Holo-Rv0203-His. The absorption spectra of the ferrous CO holoprotein adducts of Rv0203-notag and Rv0203-His are similar (Figure 4). They both feature an intense Soret peak near

dx.doi.org/10.1021/bi2018305 | *Biochemistry* 2012, 51, 1518−1531

Table 2. MCD Features of Ferric and Ferrous Holo-Rv0203-His Compared to Those of Six-Coordinate, Bis-His-Ligated Cytochrome b_5 in Both Oxidation States

protein (ref)	ligands	oxidation state	Soret (nm) [$\Delta\varepsilon/H$ (mM^{-1} cm^{-1} T^{-1})]	visible (nm) [$\Delta\varepsilon/H$ (mM^{-1} cm^{-1} T^{-1})]
Rv0203-His (this work)	His, His	Fe(III)	402 (32.2), 421 (−36.4)	551 (4.6), 570 (−5.1)
Rv0203-His (this work)	His, His	Fe(II)	430 (18.2)	549 (59.1), 558 (−60.8)
cytochrome b_5[32]	His, His	Fe(III)	405 (68.4), 418 (−98.0)	553 (9.0), 571 (−14.5)
cytochrome b_5[32]	His, His	Fe(II)	425 (15.0)	552 (160.1), 561 (−171.0)

Table 3. MCD Features of Ferric Holo-Rv0203-notag Compared to Those of Selected Five-Coordinate, Oxygen-Ligated Heme Molecules

protein (ref)	ligand	oxidation state	Soret (nm) [$\Delta\varepsilon/H$ (mM^{-1} cm^{-1} T^{-1})]	visible (nm) [$\Delta\varepsilon/H$ (mM^{-1} cm^{-1} T^{-1})]
Rv0203-notag (this work)	O	Fe(III)	398 (6.0)	527 (0), 627 (−4.2)
H93Y-Mb (pH 5.1−10.5)[38]	Tyr	Fe(III)	398 (13.2)	528 (−1.34), 621 (−10.9)
H93G-Mb (pH 10)[38]	OH^-	Fe(III)	397 (13.9)	534 (−1.94), 621 (−5.21)
Fe-PPIXDME + CH_3O^- [38]	CH_3O^-	Fe(III)	398 (13.7)	530 (−2.28), 618 (12.8)

420 nm, which is similar to that of His-Fe-CO-ligated proteins, including ferrous CO hHb[42] and the ferrous CO imidazole adduct of H93G-Mb,[40] but different from that of Tyr-Fe-CO-ligated proteins such as HasA,[43] which have a Soret peak at a lower wavelength. This suggests both carbonyl adducts of Rv0203-His and Rv0203-notag may contain a His residue as their endogenous ligand.

The MCD properties of the ferrous CO adducts of both holo-Rv0203-His and holo-Rv0203-notag are very similar to those of His-ligated myoglobin (Figure 5c) and imidazole-coordinated H93G-Mb,[40] confirming His-Fe-CO ligation under these conditions. Given the spectroscopic similarities between ferrous CO Rv0203-notag and ferrous CO Rv0203-His, it is likely that under these experimental conditions their coordination environments are equivalent.

Electron Paramagnetic Resonance (EPR) Spectroscopy of Rv0203-notag and Rv0203-His. Ferric holo-Rv0203-His displayed a mixture of $S = {}^5/_2$ and $S = {}^1/_2$ populations. The dominant species are two low-spin $S = {}^1/_2$ populations that display overlapping g = 2.8, 2.4, 2.2, and 2.0 features (Figure 6a). The high-spin species has two features at 5.8 ($g_\perp$) and 2.0 ($g_\parallel$), but it represents only a minor amount of the total heme iron. Furthermore, the high-spin population correlates with the small amount of high-spin heme detected in the absorption spectrum, which additionally suggests it corresponds to only a small percentage of the total heme species. Thus, ferric holo-Rv0203-His is predominately low-spin, which is in good agreement with its absorption spectrum (Figure 4a).

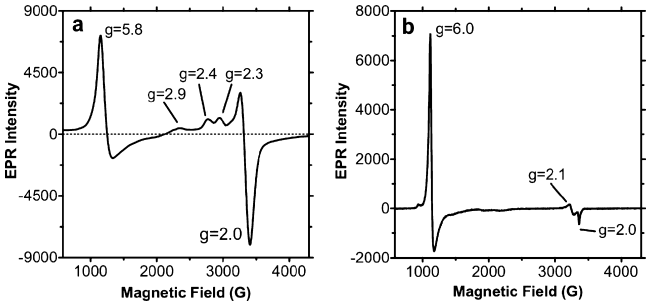

Figure 6. X-Band EPR spectra of (a) holo-Rv0203-His (440 μM) and (b) holo-Rv0203-notag (450 μM). Both proteins were in 100 mM phosphate buffer (pH 7.4). Spectra were recorded at 4.5 K, a 9.39 GHz microwave frequency, a 0.02 mW microwave power for holo-Rv0203-notag and a 10 mW microwave power for holo-Rv0203-His, a 10 G modulation amplitude, and a 100 kHz modulation frequency. The g = 2.1 feature in panel b represents a Cu(II) impurity, which was also present in a buffer-only sample.

The EPR spectrum of ferric holo-Rv0203-notag is typical of a high-spin heme protein with two g values at 6.0 ($g_\perp$) and 2.0 ($g_\parallel$) (Figure 6b). These EPR features are in agreement with the high-spin assignment based on the absorption spectrum (Figure 4b).

Y59A- and H63A/H89A-Rv0203-notag Mutants Lose Their Ability To Bind Heme. Mutagenesis experiments with Rv0203-His had demonstrated that Tyr59 is necessary for heme binding.[22] The Y59A-, Y59H-, and Y59F-Rv0203-notag mutants were produced to investigate whether this residue plays a similarly important heme binding role in Rv0203-notag.

The heme binding properties of the various mutants were compared by using a heme reconstitution experiment in which each mutant was incubated with a 1.25-fold molar excess of heme, unbound heme was removed over a desalting column, and the respective heme and protein concentrations were determined. Using this method, WT-Rv0203-notag is ∼80% heme-loaded. Y59A-Rv0203-notag, on the other hand, is unable to efficiently bind heme as only 14% of the protein forms a complex with heme after desalting (Figure 7a).

The Y59H-Rv0203-notag and Y59F-Rv0203-notag mutants are 42 and 61% heme-bound, respectively, which suggests the amount of heme bound to Rv0203-notag correlates with the hydrophobicity and amount of conjugation of the side chain of residue 59. Additionally, the difference in heme retention between WT-Rv0203-notag and the Y59F-Rv0203-notag mutant indicates the hydroxide residue contributes to heme binding, either in the form of ligation to the heme iron, or indirectly through H-bonding interactions.

Residues His63 and His89 are in the proximity of Tyr59, whereby His63 hydrogen bonds to Tyr59, and His89 is approximately 8 Å from Tyr59. Both residues are proposed to be part of the heme binding pocket for Rv0203-His.[22] Therefore, the H63A- and H89A-Rv0203-notag single mutants as well as the H63A/H89A-Rv0203-notag double mutant were produced. Both H63A-Rv0203-notag and H89A-Rv0203-notag are similarly compromised in their heme binding ability, with H63A-Rv0203-notag being 48% and H89A-Rv0203-notag being 41% heme-loaded (Figure 7a). The H63A/H89A-Rv0203-notag double mutant is severly deficient in its heme binding ability and contains 29% holoprotein (Figure 7a),

dx.doi.org/10.1021/bi2018305 | Biochemistry 2012, 51, 1518−1531

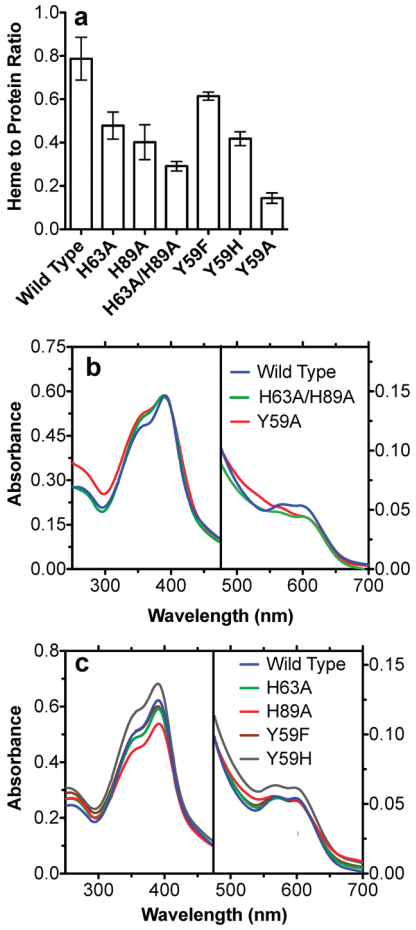

Figure 7. (a) Amount of heme loaded onto WT-Rv0203-notag compared to Rv0203-notag mutants after heme reconstitution and removal of free heme over a G-25 desalting column. Protein concentrations were determined by the modified Lowry method (Pierce) and heme concentrations using the pyridine hemochromagen assay.[28] The results represent the average of at least three independent experiments. (b) Absorption spectrum of WT-Rv0203-notag compared to those of H63A/H89A-Rv0203-notag and Y59A-Rv0203-notag. The heme concentration is 10 μM per sample. (c) Absorption spectrum of Rv0203-notag compared to those of Y59F-, Y59H-, H63A-, and H89A-Rv0203-notag mutants. All samples contain approximately 10 μM heme.

indicating that together His63 and His89 are required for efficient heme incorporation.

Absorption Spectra of Y59A-Rv0203-notag and H63A/H89A-Rv0203-notag Are Indicative of Weak, Nonspecific Binding. The Y59A-Rv0203-notag mutant displays no clear peaks in its ferric absorption spectrum between 450 and 700 nm and contains a Soret peak shoulder at 350 nm larger than that of WT-Rv0203-notag, which is indicative of nonspecific binding or of weak heme−protein interactions within the heme binding pocket (Figure 7b). In contrast, the ferric absorption spectra of the Y59H- and Y59F-Rv0203-notag mutants are nearly identical to that of WT-Rv0203-notag, suggesting the electronic environment of the heme molecule remains unchanged (Figure 7c). The similarities of the absorption spectra between Y59F-Rv0203-notag and WT-Rv0203-notag introduce the possibility that the phenolic oxygen is not coordinated to the heme iron, but rather that a hydroxide molecule occupies the fifth coordination site. Given the similarities between five-coordinate hydroxide-ligated heme compounds compared to phenolate-ligated heme, neither possibility can be excluded on the basis of these data (Table 1).

The absorption spectrum of ferric H63A/H89A-Rv0203-notag is seen in Figure 6b. It displays similarly broad features like Y59A-Rv0203-notag, which points toward nonspecific heme binding. The single mutants H63A- and H89A-Rv0203-notag on the other hand are electronically identical compared to WT-Rv0203, suggesting a very similar coordination structure (Figure 7c). Given these results, it is likely that both His63 and His89 interact with the heme molecule through noncovalent interactions but do not coordinate the heme iron.

Rv0203-notag Heme Binding Kinetics Demonstrates Fast Heme On and Off Rates. Rv0203-notag and Rv0203-His both bind heme too tightly for measurement of their heme binding affinities by direct titration. Therefore, the on rate, k_{on}, was measured by stopped flow mixing and monitoring the change in absorbance upon heme binding as a function of time. The off rate, k_{-heme}, was determined using the myoglobin assay.[30] Binding of heme to Rv0203 can be described by Scheme 1:

Scheme 1

$$\text{Rv0203 + Heme} \underset{k_{-1}}{\overset{k_1}{\rightleftharpoons}} \text{Rv0203-Heme} \underset{k_{-heme}}{\overset{k_{coord}}{\rightleftharpoons}} \text{Holo-Rv0203}$$

where Rv0203-Heme represents a weakly bound intermediate and Holo-Rv0203 is the final heme-bound protein.

When k_{-heme} is sufficiently slow and when protein is in excess, the observed pseudo-first-order rate constant, k_{obs}, is given by the hyperbolic equation (eq 1):

$$k_{obs} = \frac{k_{coord}[Rv0203]}{K_d[Rv0203]} \quad (1)$$

where $K_d = k_{-1}/k_1$. When k_{coord} is not rate-limiting, which is the case at low protein concentrations, the reaction is bimolecular and the apparent second-order association rate constant, k_{on}, is given by k_{coord}/K_d. Under these conditions, the measured rate, k_{obs}, is linearly dependent on protein concentration.[31]

To prevent heme aggregation, which would cause the reaction to become multiphasic, we measured binding of the ferrous heme carbonyl adduct to Rv0203-notag. The oxidation state of the heme group in this expeirment is not believed to affect the result because monomeric ferric cyanoheme binds with rates similar to those of ferrous CO-heme.[31,44] Binding of ferrous CO-heme to Rv0203-notag was measured at increasing protein concentrations, and the data were fit to single-exponential functions to obtain values for k_{obs} (Figure S4 of the Supporting Information). The linear slope of k_{obs} versus the concentration of the apoprotein (Figure 8a) yielded a second-order rate constant (k_{on}) of 133 ± 19 μM^{-1} s^{-1} for Rv0203-notag, which is comparable to that of several heme binding proteins (Table 4).

The off rate was measured using the apo-H64Y/V68F-myoglobin assay whereby the apomyoglobin mutant acts as a high-affinity heme scavenger.[30] The rate of the reaction depends solely on the unimolecular rate of heme release, k_{-heme}. The release of heme from ferric holo-Rv0203-notag was recorded over time (Figure S5a of the Supporting Information) and the time course fit to both single- and double-exponential functions (Figure 9a and Figure S6 of the Supporting Information). Both fitting choices produced statistically good

dx.doi.org/10.1021/bi2018305 | Biochemistry 2012, 51, 1518−1531

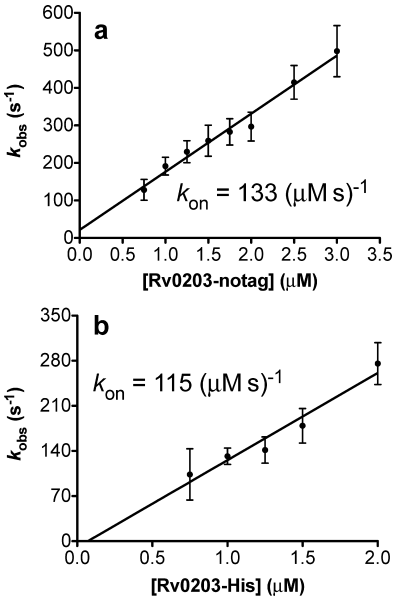

Figure 8. Plot of k_{obs} of ferrous CO-heme binding vs protein concentration to obtain the apparent second-order rate constant for binding of heme to (a) Rv0203-notag and (b) Rv0203-His.

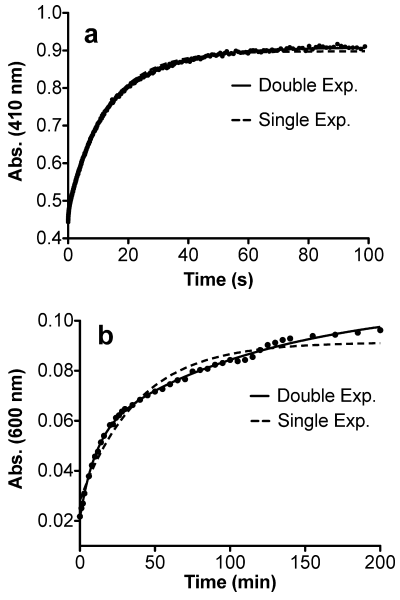

Figure 9. Time courses of transfer of heme from (a) holo-Rv0203-notag, measured at 410 nm, and (b) holo-Rv0203-His, measured at 600 nm, to a 10-fold excess amount of apo-H64Y/V68F-Mb. The exponential fitting results for holo-Rv0203-notag at 600 nm are experimentally indistinguishable from those at 410 nm and shown in Figure S6 of the Supporting Information. The experiments were conducted six times, and a representative change in absorbance vs time is shown.

results (R^2 > 98%), although the double-exponential fit produced slighty more normal residuals (Figure S7 of the Supporting Information). Fitting a single-exponential function to the data produces a k_{-heme} of 0.082 ± 0.016 s^{-1}, whereas double-exponential fitting yields a fast phase, k_f, equal to 0.77 ± 0.57 s^{-1} and a slow phase, k_s, equal to 0.05 ± 0.01 s^{-1}. There is insufficient experimental evidence to favor one model over the other. The fast and slow phases of heme release and the amplitudes of the fast and slow phases in the biphasic model do not change when the experiment is conducted with holo-Rv0203-notag that has been reconstituted with a heme:protein ratio of 0.33. This indicates that the heme off rate is not dependent on the amount of heme loading. Further, this result suggests that it is unlikely that two different heme binding sites exist, which have two different heme binding affinities. Instead, the biphasic kinetics are likely due to different conformations of Rv0203-notag, which resembles the results seen in the individual NEAT1, NEAT3, and NEAT4 domains of heme protein IsdX2 from *Bacillus anthracis*, each of which binds one heme per domain.[45] Using the value of k_{-heme} obtained from the single-exponential fit, we were able to calculate the affinity constant (K_a = 1.6 × 10^9 M^{-1}) of heme for Rv0203-notag.

Heme Binding Is Slightly Slowed for all Rv0203-notag Mutants. To compare the relative rates of heme binding between WT-Rv0203-notag and the Rv0203-notag mutants, 1 μM ferrous CO-heme was rapidly mixed with 2 μM apo-Rv0203-notag and the observed rate constant, k_{obs}, determined by single-exponential fitting of the experimental binding curve (Table 5). Because the value of k_{obs} is expected to differ depending on the respective on rate, k_{on}, k_{obs} serves as an

Table 4. Kinetic Parameters for Binding of Heme to Selected Heme Proteins

protein (ref)	k_{on} (μM^{-1} s^{-1})	k_{-heme} (s^{-1})	K_a (M^{-1})	method
Rv0203-notag (this work)	133 ± 19	single exponential, (8.2 ± 1.6) × 10^{-2}	1.6 × 10^9 (single exponential)	stopped flow
		double exponential, k_f (22%), 7.7 × 10^{-1} ± 5.7 × 10^{-2}; k_s, (5 ± 1) × 10^{-2}		
Rv0203-His (this work)	115 ± 30	k_f (31%), 1.9 × 10^{-3} ± 6 × 10^{-4}; k_s, (2 ± 1) × 10^{-4}	5.8 × 10^{11} M^{-1} (using slow phase for k_{-heme})	stopped flow
Mb[31]	70	8.4 × 10^{-7}	8 × 10^{13}	stopped flow
H93G-Mb[31]	70	1.2 × 10^{-2}	6 × 10^9	stopped flow
BSA[31]	~50	1.1 × 10^{-2}	4 × 10^9	stopped flow
IsdA[46]	100	2.6 × 10^{-4}	3.8 × 10^{11}	stopped flow
IsdB[47]		k_f 2.8 × 10^{-2}; k_s, 4.2 × 10^{-3}	>2.6 × 10^6	stopped flow, fluorescence titration
Shp[48]	1.6	3 × 10^{-4}	5.3 × 10^9	stopped flow
HtsA[48]	80	2.6 × 10^{-3}	3.1 × 10^{10}	stopped flow
HasA[15,25]	16	3 × 10^{-4} (calcd from k_{-heme} = k_{on}/K_a)	5.3 × 10^{10}	stopped flow, ITC
PhuS[49]	0.18 (calcd from k_{on} = $K_a k_{-heme}$)	3.6 × 10^{-2}	5.0 × 10^6	fluorescence titration
HmuT[50]			3.4 × 10^9 (first heme molecule)	ITC

dx.doi.org/10.1021/bi2018305 | *Biochemistry* 2012, 51, 1518–1531

Table 5. Off Rates and k_{obs} Values for the Rv0203-notag Mutants Compared to Those of WT-Rv0203-notag

	single-exponential k_{-heme} (s^{-1})	double-exponential k_f and k_s (s^{-1})	k_{obs} (s^{-1})
Y59F	0.094 ± 0.02	k_f, 1.2 ± 0.5 (15 ± 5%); k_s, 0.07 ± 0.0	87 ± 17
Y59H	0.1 ± 0.03	k_f, 0.95 (30%); k_s, 0.06	82 ± 37
Y59A	0.367 ± 0.069	k_f, 2.15 ± 0.78 (36 ± 15%); k_s, 0.07 ± 0.04	82 ± 24
H63A	0.0896 ± 0.028	k_f, 0.3 ± 0.14 (30 ± 2%); k_s, 0.04 ± 0.01	109 ± 8
H89A	0.114 ± 0.037	k_f, 0.92 ± 0.27 (27 ± 0%); k_s, 0.08 ± 0.02	80 ± 9
H63A/H89A	0.234 ± 0.072	k_f, 2.01 ± 1.15 (28 ± 9%); k_s, 0.08 ± 0.056	not available
WT	0.082 ± 0.16	k_f, 0.77 ± 0.57 (22 ± 6%); k_s, 0.05 ± 0.01	126 ± 13
H64Y/V58F-Mb with ferric heme	1.8 (ferric heme binding)	k_f, 4.5 (42%); k_s, 0.13 (ferric heme binding)	

estimate for comparing heme binding rates between mutants. The values of k_{obs} are slightly slower compared to that of the wild type for all Rv0203-notag mutants, in line with the evidence that each mutant is less capable of binding heme than WT-Rv0203-notag (Figure 7a). Besides binding heme slower, the reaction amplitudes for both Y59H- and Y59A-Rv0203 are approximately 40−50% lower than for WT-Rv0203-notag (data not shown), which suggests ferrous CO-heme incorporation is incomplete under the experimental conditions. Binding of ferrous CO-heme to H63A/H89A-Rv0203-notag was not measured because the ferrous CO absorption spectrum of this mutant indicates nearly all heme is present as free ferrous CO-heme.

Heme Release Is Fast for H63A/H89A-Rv0203-notag and Y59A-Rv0203-notag. The kinetic parameter determining the heme binding affinity is off rate k_{-heme}. Therefore, the heme off rate of each Rv0203-notag mutant was measured using the apo-H64Y/V68F-Mb assay. As seen in Figure 10a, the release of heme from Y59A- and H63A/H89A-Rv0203-notag occurs faster than that from WT-Rv0203-notag. A double-exponential fit describes the data better for Y59A- and H63A/H89A-Rv0203-notag because the single-exponential fitting results cannot be used to model both the rapid heme release in the early parts of the reaction and the later slower stage of heme release (Figure 10a). The rate constants, k_{-heme}, for Y59A- and H63A/H89A-Rv0203-notag using either single- or double-exponential fitting are faster for both mutants than for the wild type. In fact, when using the double-exponential fitting results, the rate of release of heme from the Y59A- and H63A/H89A-Rv0203-notag mutants is approximately half as fast as the rate of binding of ferric free heme to apo-H64Y/V68F-Mb under the same conditions (Table 5). This indicates that the faster dissociation kinetics is likely due to heme having dissociated from these mutants prior to the experiment or due to nonspecifically bound heme, which yields similarly rapid heme off rates.[31]

The rates of release of heme from the H63A-, H89A-, Y59H-, and Y59F-Rv0203-notag mutants are quite similar to that of WT protein (Figure 10b). As with WT-Rv0203-notag, both single- and double-exponential functions fit the data, and the results for both fitting choices are listed in Table 5.

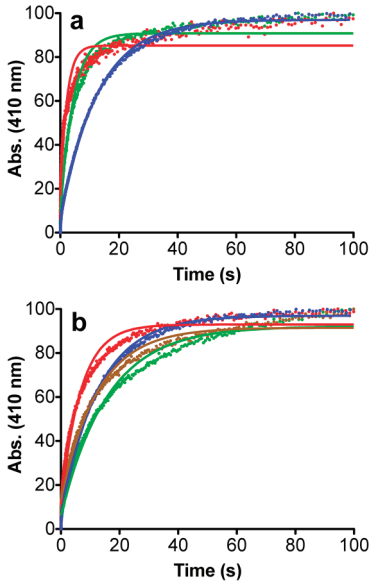

Figure 10. (a) Time courses of dissociation of heme from Y59A-Rv0203-notag (red), H63A/H89A-Rv0203-notag (green), and WT-Rv0203-notag (blue) and single-exponential fitting results. (b) Time course for dissociation of heme from H63A-Rv0203-notag (green), H89A-Rv0203-notag (red), and Y59F-Rv0203-notag (brown) compared to that from WT-Rv0203-notag (blue) and single-exponential fitting curves. The data were normalized to account for the different amounts of heme per sample, as explained in Materials and Methods.

Interestingly, using a double-exponential fit, the fast phase of k_{-heme} for H63A-Rv0203-notag is slower than that of WT-Rv0203-notag. However, the difference falls within the experimental error for the fast phase of release of heme of WT-Rv0203-notag and therefore is unlikely to be relevant.

Rv0203-His Has a Heme Binding Affinity Higher Than That of Rv0203-notag. The heme binding affinity of Rv0203-His was measured like that of Rv0203-notag. The rate k_{on} is 115 ± 30 μM^{-1} s^{-1}, which is similar to that of Rv0203-notag (Figure 8b). Unlike the case for Rv0203-notag, fitting the heme dissociation kinetics requires a biphasic fit, as judged by the residuals (Figure S8 of the Supporting Information). Using a biphasic model, the fast phase of k_{-heme} is equal to 0.0019 ± 0.0006 s^{-1} and the slow phase is equal to 0.0002 ± 0.0001 s^{-1} (Figure 9b and Figure S5b of the Supporting Information). The K_a for Rv0203-His, using the slow phase for k_{-heme}, is equal to 5.8×10^{11} M^{-1}, thus indicating the heme binding affinity is approximately 2 orders of magnitude higher for Rv0203-His than for Rv0203-notag (Table 4).

DISCUSSION

The His Tag of Rv0203-His Interferes with Heme Binding. Previous mutational analysis of Rv0203-His identified residue Tyr59 as being essential for heme binding, whereas H63A and H89A single mutations did not abolish heme binding and displayed ferric absorption spectra similar to those of WT-Rv0203-His (Figure S9 of the Supporting Information).[22] In this study, the combined results from absorption, EPR, and MCD spectra of Rv0203-His suggest that the heme iron is low-spin and coordinated through two His residues (Tables 1 and 2). This assignment is supported by the Rv0203-His absorption spectrum that does not contain a charge transfer band typical of tyrosine ligation near or above 600 nm (Table 1), and the MCD features of Rv0203-His that are dissimilar to

dx.doi.org/10.1021/bi2018305 | Biochemistry 2012, 51, 1518−1531

those of hydroxide or Tyr-coordinated heme proteins[36,38] (Table 3) but similar to those of bis-His-ligated heme proteins (Table 2). The EPR spectrum of Rv0203-notag suggests the heme iron is high-spin and the absorption and MCD spectra of Rv0203-notag indicate the predominant axial ligand to the heme iron is anionic oxygen. Thus, we have conflicting biophysical results for the ligation of the heme iron between Rv0203-His and Rv0203-notag. The biophysical evidence leads one to speculate that the second His ligand to holo-Rv0203-His is donated by the His tag. From the structure of apo-Rv0203-His, His63 and His89 are located in a solvent accessible cleft approximately 16 Å from the N-terminus of an adjacent subunit, whereby the flexible 15-amino acid N-terminal tag (including the hexahistidine tag) could feasibly bridge this gap to ligate the heme iron (Figure 1). To date, there is only one well-documented case of His tag interference with heme binding. Within the cytochrome *c* maturation protein, CcmE, heme is pentacoordinated through His130,[51,52] whereas in the presence of a His tag, heme binding is bis-His-hexacoordinated, suggesting one His is provided by the tag.[53,54] The heme binding sites of both Rv0203-His and CcmE are both surface-exposed, which suggests that His tag interference can occur when the heme group is solvent accessible in conjunction with the heme group being in the proximity of the His tag.

Analysis of Heme Coordination for Rv0203-notag and Rv0203-His. The absorption spectra of both ferric and ferrous Rv0203-notag (Figure 4b) and the ferric Rv0203-notag EPR spectrum are indicative of high-spin heme molecules (Figure 6b). The relatively blue-shifted position of the Soret peak in the absorption spectrum could indicate coordination through an anionic oxygen or cysteine ligand. The MCD spectrum of Rv0203-notag (Figure 5b) most closely resembles those of oxygen-ligated heme molecues. The possibility of Cys ligation can be excluded on the basis of two observations. First, there are only two cysteine residues within Rv0203, and from the crystal structure of apo-Rv0203, they form a disulfide bond.[22] Second, the ferric MCD spectra of Cys-ligated heme proteins display strong negative features in the Soret region,[39] which are not observed in the MCD spectrum of holo-Rv0203-notag. Because the nature of the axial ligand was not evident from the spectrosocopic evidence alone, a mutational analysis within the proposed heme binding site was conducted. The Y59A-Rv0203-notag mutant provides the strongest evidence that this residue is required for heme binding. This mutant does not bind heme efficiently, features a rapid rate for $k_{-\text{heme}}$, similar to that of nonspecifically bound or free heme, and has a poorly resolved absorption spectrum (Figures 7 and 10). This result mirrors what was observed for Rv0203-His.[22] Furthermore, the presence of a Tyr residue in the heme binding site would resemble that of many heme transporters and hemophores, including HasA,[24] PhuT,[55] and the NEAT domain family of heme proteins.[12,56,57] This propensity for Tyr is intriguing because very few heme proteins contain Tyr ligands other than heme transport-type proteins. It is possible that the commonality of Tyr ligands in bacterial heme transport proteins is due to its preference for ferric metal, which is the oxidation state of heme within the most abundant host heme source, met-hemoglobin.[11] The experimental evidence indicates that the most important characteristic of residue 59 is its ability to form $\pi-\pi$ stacking interactions with the heme group. The Y59F-Rv0203-notag mutant is relatively uncompromised in its ability to bind heme, has an off rate, $k_{-\text{heme}}$, similar to that of the wild type, and displays little spectral difference compared to ferric wild-type Rv0203-notag, all of which suggests the availability of a phenol ring at position 59 is critical for heme binding (Figures 7 and 10).

Despite the evidence supporting oxygen ligation, the exact coordination structure of WT-Rv0203-notag cannot be conclusively inferred from these data. On one hand, the heme reconstitution assay indicates the hydroxyl group of Tyr59 is required for complete incorporation of heme into Rv0203-notag, which could indicate the hydroxyl group coordinates to the metal. On the other hand, the similar ferric absorption spectra of WT-Rv0203-notag and Y59F-Rv0203-notag indicate the oxygen ligand may be in the form of an exogenous hydroxide molecule. We cannot distinguish either possibility because an exogenous hydroxide molecule can substitute for the tryosinate hydroxyl group in the Y59F-Rv0203-notag mutant, and the absorption spectra of Tyr- and OH^--ligated heme groups are known to be very similar. If hydroxide is the sole heme ligand, as suggested for Y59F-Rv0203-notag, it would resemble the ligation mode of the myoglobin mutant H93G-Mb.[38] In the case of H93G-Mb, heme is bound to the protein through noncovalent interactions between the heme group and the residues surrounding the heme binding pocket.[31]

Rv0203-notag residues His63 and His89 have been shown to be critical for tight heme binding. For H63A-, H89A-, and H63A/H89A-Rv0203-notag mutants, the off rates increase, while the values for k_{obs} decrease slightly for both single mutants (Table 5). Furthermore, the H63A/H89A-Rv0203-notag double mutant displays a poorly resolved ferric absorption spectrum. Therefore, these residues likely constitute, with Tyr59, the heme binding pocket. It is, however, very unlikely that His63 and His89 bind to the heme iron because the MCD spectrum of Rv0203-notag does not resemble those of high-spin His-coordinated heme proteins, which lack the derivative-shaped feature in the visible region seen in Rv0203-notag[40,58] (Tables 2 and 3). Moreover, the H63A/H89A-Rv0203-notag double mutant, although unable to bind heme well, retains more heme than the Y59A-Rv0203-notag single mutant, which suggests neither His residue is as critical in heme binding as is Tyr59. Instead, His63 and His89 likely interact noncovalently with the heme group. As such, residues His63 and His89 may fulfill roles similar to those of the His and Tyr residues surrounding the heme binding site of NEAT domain heme binding proteins. While all NEAT domain proteins coordinate heme through a conserved Tyr residue, additional His and Tyr residues are present to form electrostatic and $\pi-\pi$ stacking interactions with the heme group.[12,56,57]

The roles of His63 and His89 in heme binding are different between Rv0203-His and Rv0203-notag. Rv0203-His is hexacoordinate, where one His ligand is donated by either His63 or His89 and the other by the His tag. In Rv0203-His, the heme binding pocket therefore contains coordination redundancy. This is also the case for the periplasmic heme transporter PhuS from *Pseudomonas aeruginosa*.[59] PhuS presents two His residues, His209 and His212, to one face of the heme molecule, with His209 being the physiological ligand. An H209A mutant results in recovery of heme binding by His212. The PhuS heme binding site further contains His210, which does not coordinate to the heme iron, but its presence is required for complete loading of heme onto PhuS as it forms hydrogen bond interactions with both possible heme ligands. In Rv0203-His, either His63 or His89 may assume the role of His209 of PhuS, whereby the H63A and H89A single

dx.doi.org/10.1021/bi2018305 | *Biochemistry* 2012, 51, 1518−1531

mutations of Rv0203-His do not abolish heme binding because either residue can coordinate the heme molecule in the absence of the other.

The carbonyl adducts for both Rv0203-His and Rv0203-notag ligate heme through an endogenous His residue. This indicates that for Rv0203-notag a switch of the ligand from an oxygen ligand to a nitrogen ligand must occur during reduction or because of CO binding trans of the fifth ligand. A ligand switch in favor of His upon reduction has been reported when ferric heme has a oxygen ligand, as in the myoglobin mutant H93Y-Mb[37] and *Chlamydomonas* hemoglobin.[60] The endogenous His coordination of the carbonyl adduct further supports the hypothesis that the heme binding site consists of Tyr59, His63, and His89.

Implication of Differences in k_{obs} and k_{-heme} across Rv0203-notag Mutants for the Heme Binding Mechanism. The differences in heme loading between WT-Rv0203-notag and the H63A-Rv0203-notag mutant are most likely due to different on rates because their respective off rates are nearly identical. Similarly, the Y59F-, Y59H-, and H89A-Rv0203-notag mutants have slightly slower values for k_{obs} and feature a small increase in k_{-heme}, which suggests both on and off rates cause the reduced heme binding capabilities. In the case of Y59A- and H63A/H89A-Rv0203-notag, both the k_{obs} and to a greater extent the off rate are affected for both mutants, implying that these mutants are compromised in both their heme binding and heme retention capabilities (Figure 10 and Table 5). The significantly higher values of k_{-heme} for Y59A- and H63A/H89A-Rv0203-notag indicate these mutants contain loosely coordinated heme in the heme binding pocket or, alternatively, heme is nonspecifically bound. Considering the poorly resolved ferric absorption spectra (Figure 7b), the later possibility is more likely. It is unclear why release of heme from H63A/H89A- and Y59A-Rv0203-notag mutants appears to be biphasic, but it is reasonable to postulate that more than one site where heme binds nonspecifically exists. The larger differences in heme off rates compared to on rates between Rv0203-notag heme binding site mutants are in line with obervations from mutational analyses within heme binding sites of other heme binding proteins.[15,31]

The lack of large differences between Rv0203-notag mutants in the rates of k_{obs} can be explained by the fact that heme binding is a two-step mechanism (scheme 1) where, under the experimental conditions, the formation of the Rv0203−heme intermediate is rate-limiting. Because the overall heme binding pocket structure is unlikely to be very different between mutants, k_{obs} is not expected to vary depending on the mutant. The second step in binding, the formation of holo-Rv0203, involves binding pocket rearrangements[31] and may be more variable between the Rv0203-notag mutants. However, we could not determine the rate governing the second heme binding step, k_{coord}, because we were unable to measure heme binding when the amount of apoprotein is in large excess compared to the heme concentration, which is the required condition for measurement of k_{coord}.

Heme Binding Affinities and Functional Implications. The on rates of Rv0203-notag (133 μM^{-1} s^{-1}) and Rv0203-His (115 μM^{-1} s^{-1}) are similar to those of several heme proteins, including myoglobin,[31] the heme transporter IsdA,[46] and the heme receptor HtsA[48] (Table 4). Rv0203-notag features a fast rate of heme release (0.082 s^{-1}), similar to those of BSA and H93G-Mb[31] and the heme transport domain of IsdB, IsdB-N2.[47] Because of the relatively fast off rate, the K_a for Rv0203-notag (1.6×10^9 M^{-1}) is lower than that of the hemophore HasA.[25] It is comparable to those of IsdB-N2,[47] the myoglobin cavity mutant H93G-Mb, BSA,[31] the *Streptococcus pyogenes* cell surface heme transporter Shp,[48] and the *Yersinia pestis* periplasmic heme transporter HmuT[50] (Table 4). The heme binding affinities of Rv0203-His and Rv0203-notag differ; the respective K_a for Rv0203-His is 5.8×10^{11} M^{-1} (using the slow phase for k_{-heme}) (Table 4). The higher affinity of Rv0203-His could be due to the second axial ligand donated by the His tag representing a higher kinetic barrier for heme release or additional noncovalent interactions between the His tag and the heme group.

The lower heme binding constant of Rv0203-notag compared to that of the known hemophore HasA (Table 4) suggests that Rv0203-notag is not able to acquire heme from hemoglobin based on an affinity gradient. Instead, its K_a falls into the range of those of several heme transport proteins such as the heme periplasmic trafficking proteins PhuS[49] and HmuT[50] that bind heme with affinities of 5.0×10^6 and 3.4×10^9 M^{-1}, respectively, and BSA, an important heme trafficking protein in the bloodstream, which binds free heme with a K_a of 4×10^9 M^{-1}.[31] Taken together, the fast off rate and the similarities in heme binding affinity with BSA and other heme transport proteins may indicate that Rv0203-notag functions as a heme transporter. We previously proposed that the transmembrane proteins, MmpL3 and MmpL11, which have been shown to play a role in heme uptake,[22] are heme receptors and may interact with heme-bound Rv0203. Both proteins contain predicted extracellular domains, which bind heme and may facilitate the transport of heme across the mycobacterial membrane.

CONCLUSIONS

The results of this work suggest that the heme binding site of Rv0203 consists of Tyr59, His63, and His89. Furthermore, Tyr59 appears to play a key role in heme iron ligation during in vitro heme reconstitution of both Rv0203-His and Rv0203-notag. The different heme coordination structures between holo-Rv0203-notag and holo-Rv0203-His raise the question of how the His tag creates bis-His heme ligation when holo-Rv0203-notag is most likely oxygen-ligated. The Y59A-Rv0203-His mutant does not bind heme.[22] Therefore, it is likely that heme binding in Rv0203-His is initiated through the action of residue Tyr59 to form a five-coordinate heme structure in a mechanism similar to heme binding in Rv0203-notag. Once the heme group is located in the heme binding pocket of Rv0203-His, the His tag may bind to the open face of the heme molecule, thus changing the structural and electronic properties of the heme group and inducing a trans ligand switch from an oxygen to either His63 or His89. The observations that either His63 or His89 can bind heme in Rv0203-His and that both residues are important for full heme incorporation in Rv0203-notag lead to the hypothesis that these histidine residues could play a major role in the transfer of heme from a host hemoprotein to the mycobacterial heme receptor. Rv0203 is a mycobacterially specific, secreted heme binding protein involved in mycobacterial heme uptake.[22] This work offers the first insights into the heme binding properties of Rv0203 and sets the stage for the development of inhibitors against this new pathway of heme iron uptake in Mtb.

dx.doi.org/10.1021/bi2018305 | *Biochemistry* 2012, 51, 1518−1531

■ ASSOCIATED CONTENT

Supporting Information

UV−vis absorption spectra of ferricyanide-treated holo-Rv0203-notag and holo-Rv0203-His and the size exclusion chromotography traces for holo- and apo-Rv0203-notag, ferrous holo-Rv0203-notag in a 1:1 complex with heme, time courses of binding of ferrous CO-heme to apo-Rv0203-notag with single-exponential fitting results, time-resolved absoption spectra of heme dissociation of ferric holo-Rv0203-notag and ferric holo-Rv0203-His, experimental data and single-exponential fitting of the apomyoglobin data for Rv0203-notag measured at 600 nm and the residual plots for both single- and double-exponential fitting of the apomyoglobin data for Rv0203-notag and Rv0203-His, and ferric absorption spectra of holo-H63A-, H89A-, and WT-Rv0203-His. This material is available free of charge via the Internet at http://pubs.acs.org.

■ AUTHOR INFORMATION

Corresponding Author

*Department of Molecular Biology and Biochemistry and Department of Pharmaceutical Sciences, University of California, Irvine, CA 92697. Telephone: (949) 824-0337. E-mail: celia.goulding@uci.edu.

Funding

This work has been supported by a grant from the National and Californian American Lung Association (RG-78755-N to C.W.G.) and the National Institutes of Health (Grant AI081161 to C.W.G. and Grant GM26730 to J.H.D.).

Notes

The authors declare no competing financial interests.

■ ACKNOWLEDGMENTS

We thank Dr. Masanori Sono and Shengfang Sun (University of South Carolina) and Pat Farmer (University of California, Irvine) for useful discussions. We also thank Drs. Tom Poulos and Nick Chim for critical reading of the manuscript and Dr. Nick Chim, Guneet Singh, and Evgeny Fadeev for assistance with the experiments. John Olsen kindly provided the clone to produce the H64Y/V68F-Mb mutant. We also thank the reviewers of this paper for their helpful and insightful comments.

■ ABBREVIATIONS

BME, β-mercaptoethanol; BSA, bovine serum albumin; EPR, electron paramagnetic resonance; far-UV CD, far-ultraviolet circular dichroism; Fe-PPIXDME, Fe-protoporphyrin IX dimethyl ester; hHb, human hemoglobin; hHO, human heme oxygenase; hMb, human myoglobin; HRP, horseradish peroxidase; ITC, isothermal titration calorimetry; Mb, myoglobin; MCD, magnetic circular dichroism; NCBI, National Center for Biotechnology Information; OD, opitcal density; SDS−PAGE, sodium dodecyl sulfate−polyacrylamide gel electrophoresis; swMb, sperm whale myoglobin.

■ REFERENCES

(1) World Health Organization (2011) 2011/2012 Tuberculosis Global Facts.

(2) Gobin, J., and Horwitz, M. A. (1996) Exochelins of *Mycobacterium tuberculosis* remove iron from human iron-binding proteins and donate iron to mycobactins in the *M. tuberculosis* cell wall. *J. Exp. Med. 183*, 1527−1532.

(3) Ratledge, C. (2004) Iron, mycobacteria and tuberculosis. *Tuberculosis 84*, 110−130.

(4) Snow, G. A. (1970) Mycobactins: Iron-chelating growth factors from mycobacteria. *Bacteriol. Rev. 34*, 99−125.

(5) Rodriguez, G. M., and Smith, I. (2006) Identification of an ABC transporter required for iron acquisition and virulence in *Mycobacterium tuberculosis*. *J. Bacteriol. 188*, 424−430.

(6) Rodriguez, G. M. (2006) Control of iron metabolism in *Mycobacterium tuberculosis*. *Trends Microbiol. 14*, 320−327.

(7) Johnson, E. E., Srikanth, C. V., Sandgren, A., Harrington, L., Trebicka, E., Wang, L., Borregaard, N., Murray, M., and Cherayil, B. J. (2010) Siderocalin inhibits the intracellular replication of *Mycobacterium tuberculosis* in macrophages. *FEMS Immunol. Med. Microbiol. 58*, 138−145.

(8) Skaar, E. P., Humayun, M., Bae, T., DeBord, K. L., and Schneewind, O. (2004) Iron-source preference of *Staphylococcus aureus* infections. *Science 305*, 1626−1628.

(9) Hagan, E. C., and Mobley, H. L. (2009) Haem acquisition is facilitated by a novel receptor Hma and required by uropathogenic *Escherichia coli* for kidney infection. *Mol. Microbiol. 71*, 79−91.

(10) Mazmanian, S. K., Skaar, E. P., Gaspar, A. H., Humayun, M., Gornicki, P., Jelenska, J., Joachmiak, A., Missiakas, D. M., and Schneewind, O. (2003) Passage of heme-iron across the envelope of *Staphylococcus aureus*. *Science 299*, 906−909.

(11) Zhu, H., Xie, G., Liu, M., Olson, J. S., Fabian, M., Dooley, D. M., and Lei, B. (2008) Pathway for heme uptake from human methemoglobin by the iron-regulated surface determinants system of *Staphylococcus aureus*. *J. Biol. Chem. 283*, 18450−18460.

(12) Grigg, J. C., Ukpabi, G., Gaudin, C. F., and Murphy, M. E. (2010) Structural biology of heme binding in the *Staphylococcus aureus* Isd system. *J. Inorg. Biochem. 104*, 341−348.

(13) Honsa, E. S., and Maresso, A. W. (2011) Mechanisms of iron import in anthrax. *BioMetals 24*, 533−545.

(14) Izadi, N., Henry, Y., Haladjian, J., Goldberg, M. E., Wandersman, C., Delepierre, M., and Lecroisey, A. (1997) Purification and characterization of an extracellular heme-binding protein, HasA, involved in heme iron acquisition. *Biochemistry 36*, 7050−7057.

(15) Yukl, E. T., Jepkorir, G., Alontaga, A. Y., Pautsch, L., Rodriguez, J. C., Rivera, M., and Moenne-Loccoz, P. (2010) Kinetic and Spectroscopic Studies of Hemin Acquisition in the Hemophore HasAp from *Pseudomonas aeruginosa*. *Biochemistry 49*, 6646−6654.

(16) Cescau, S., Cwerman, H., Letoffe, S., Delepelaire, P., Wandersman, C., and Biville, F. (2007) Heme acquisition by hemophores. *BioMetals 20*, 603−613.

(17) Wandersman, C., and Delepelaire, P. (2004) Bacterial iron sources: From siderophores to hemophores. *Annu. Rev. Microbiol. 58*, 611−647.

(18) Lewis, J. P., Dawson, J. A., Hannis, J. C., Muddiman, D., and Macrina, F. L. (1999) Hemoglobinase activity of the lysine gingipain protease (Kgp) of *Porphyromonas gingivalis* W83. *J. Bacteriol. 181*, 4905−4913.

(19) Otto, B. R., van Dooren, S. J., Nuijens, J. H., Luirink, J., and Oudega, B. (1998) Characterization of a hemoglobin protease secreted by the pathogenic *Escherichia coli* strain EB1. *J. Exp. Med. 188*, 1091−1103.

(20) Yongqing, T., Potempa, J., Pike, R. N., and Wijeyewickrema, L. C. (2011) The lysine-specific gingipain of *Porphyromonas gingivalis*: Importance to pathogenicity and potential strategies for inhibition. *Adv. Exp. Med. Biol. 712*, 15−29.

(21) Tullius, M. V., Harth, G., Maslesa-Galic, S., Dillon, B. J., and Horwitz, M. A. (2008) A Replication-Limited Recombinant *Mycobacterium bovis* BCG vaccine against tuberculosis designed for human immunodeficiency virus-positive persons is safer and more efficacious than BCG. *Infect. Immun. 76*, 5200−5214.

(22) Tullius, M. V., Harmston, C. A., Owens, C. P., Chim, N., Morse, R. P., McMath, L. M., Iniguez, A., Kimmey, J. M., Sawaya, M. R., Whitelegge, J. P., Horwitz, M. A., and Goulding, C. W. (2011) Discovery and characterization of a unique mycobacterial heme acquisition system. *Proc. Natl. Acad. Sci. U.S.A. 108*, 5051−5056.

(23) Jones, C. M., and Niederweis, M. (2011) *Mycobacterium tuberculosis* can utilize heme as an iron source. *J. Bacteriol. 193*, 1767−1770.
(24) Arnoux, P., Haser, R., Izadi, N., Lecroisey, A., Delepierre, M., Wandersman, C., and Czjzek, M. (1999) The crystal structure of HasA, a hemophore secreted by *Serratia marcescens*. *Nat. Struct. Biol. 6*, 516−520.
(25) Deniau, C., Gilli, R., Izadi-Pruneyre, N., Létoffé, S., Delepierre, M., Wandersman, C., Briand, C., and Lecroisey, A. (2003) Thermodynamics of Heme Binding to the HasASM Hemophore: Effect of Mutations at Three Key Residues for Heme Uptake. *Biochemistry 42*, 10627−10633.
(26) Goulding, C. W., and Perry, L. J. (2003) Protein production in *Escherichia coli* for structural studies by X-ray crystallography. *J. Struct. Biol. 142*, 133−143.
(27) Dawson, J. H., Elliot, D. C., Elliot, W. H., and Jones, K. M. (1986) *Data for Biochemical Research*, Oxford University Press, Oxford, U.K.
(28) Bartsch, R. G. (1971) Cytochromes: Bacterial. *Methods Enzymol. 23*, 344−363.
(29) Huff, A. M., Chang, C., Cooper, D., Smith, K., and Dawson, J. H. (1993) Imidazole- and alkylamine-ligated iron(II,III) chlorin complexes as models for histidine and lysine coordination to iron in dihydroporphyrin-containing proteins: Characterization with magnetic circular dichroism spectroscopy. *Inorg. Chem. 32*, 1460−1466.
(30) Hargrove, M. S., Singleton, E. W., Quillin, M. L., Ortiz, L. A., Phillips, G. N. Jr., Olson, J. S., and Mathews, A. J. (1994) His64(E7)→Tyr apomyoglobin as a reagent for measuring rates of hemin dissociation. *J. Biol. Chem. 269*, 4207−4214.
(31) Hargrove, M. S., Barrick, D., and Olson, J. S. (1996) The Association Rate Constant for Heme Binding to Globin Is Independent of Protein Structure. *Biochemistry 35*, 11293−11299.
(32) Cheek, J., Mandelman, D., Poulos, T. L., and Dawson, J. H. (1999) A study of the K^+-site mutant of ascorbate peroxidase: Mutations of protein residues on the proximal side of the heme cause changes in iron ligation on the distal side. *J. Biol. Inorg. Chem. 4*, 64−72.
(33) Uno, T., Ryu, D., Tsutsumi, H., Tomisugi, Y., Ishikawa, Y., Wilkinson, A. J., Sato, H., and Hayashi, T. (2004) Residues in the distal heme pocket of neuroglobin. Implications for the multiple ligand binding steps. *J. Biol. Chem. 279*, 5886−5893.
(34) Caillet-Saguy, C., Turano, P., Piccioli, M., Lukat-Rodgers, G. S., Czjzek, M., Guigliarelli, B., Izadi-Pruneyre, N., Rodgers, K. R., Delepierre, M., and Lecroisey, A. (2008) Deciphering the structural role of histidine 83 for heme binding in hemophore HasA. *J. Biol. Chem. 283*, 5960−5970.
(35) Liu, Y., Moenne-Loccoz, P., Hildebrand, D. P., Wilks, A., Loehr, T. M., Mauk, A. G., and Ortiz de Montellano, P. R. (1999) Replacement of the Proximal Histidine Iron Ligand by a Cysteine or Tyrosine Converts Heme Oxygenase to an Oxidase. *Biochemistry 38*, 3733−3743.
(36) Ghosh, K., Thompson, A. M., Goldbeck, R. A., Shi, X., Whitman, S., Oh, E., Zhiwu, Z., Vulpe, C., and Holman, T. R. (2005) Spectroscopic and Biochemical Characterization of Heme Binding to Yeast Dap1p and Mouse PGRMC1p. *Biochemistry 44*, 16729−16736.
(37) Egeberg, K. D., Springer, B. A., Martinis, S. A., Sligar, S. G., Morikis, D., and Champion, P. M. (1990) Alteration of sperm whale myoglobin heme axial ligation by site-directed mutagenesis. *Biochemistry 29*, 9783−9791.
(38) Pond, A. E., Roach, M. P., Sono, M., Rux, A. H., Franzen, S., Hu, R., Thomas, M. R., Wilks, A., Dou, Y., Ikeda-Saito, M., Ortiz de Montellano, P. R., Woodruff, W. H., Boxer, S. G., and Dawson, J. H. (1999) Assignment of the Heme Axial Ligand(s) for the Ferric Myoglobin (H93G) and Heme Oxygenase (H25A) Cavity Mutants as Oxygen Donors Using Magnetic Circular Dichroism. *Biochemistry 38*, 7601−7608.
(39) Qin, J., Perera, R., Lovelace, L. L., Dawson, J. H., and Lebioda, L. (2006) Structures of Thiolate- and Carboxylate-Ligated Ferric H93G Myoglobin: Models for Cytochrome P450 and for Oxyanion-Bound Heme Proteins. *Biochemistry 45*, 3170−3177.
(40) Pond, A. E., Roach, M. P., Thomas, M. R., Boxer, S. G., and Dawson, J. H. (2000) The H93G myoglobin cavity mutant as a versatile template for modeling heme proteins:Ferrous, ferric, and ferryl mixed-ligand complexes with imidazole in the cavity. *Inorg. Chem. 39*, 6061−6066.
(41) Tang, Q., Kalsbeck, W. A., Olson, J. S., and Bocian, D. F. (1998) Disruption of the heme iron-proximal histidine bond requires unfolding of deoxymyoglobin. *Biochemistry 37*, 7047−7056.
(42) Antonini, E., and Brunori, M. (1971) *Hemoglobin and Myoglobin in their Reactions with Ligands*, North-Holland Publishers, Amsterdam.
(43) Lukat-Rodgers, G. S., Rodgers, K. R., Caillet-Saguy, C., Izadi-Pruneyre, N., and Lecroisey, A. (2008) Novel Heme Ligand Displacement by CO in the Soluble Hemophore HasA and Its Proximal Ligand Mutants: Implications for Heme Uptake and Release. *Biochemistry 47*, 2087−2098.
(44) Kawamura-Konishi, Y., Kihara, H., and Suzuki, H. (1988) Reconstitution of myoglobin from apoprotein and heme, monitored by stopped-flow absorption, fluorescence and circular dichroism. *Eur. J. Biochem. 170*, 589−595.
(45) Honsa, E. S., Fabian, M., Cardenas, A. M., Olson, J. S., and Maresso, A. W. (2011) The five near-iron transporter (NEAT) domain anthrax hemophore, IsdX2, scavenges heme from hemoglobin and transfers heme to the surface protein IsdC. *J. Biol. Chem. 286*, 33652−33660.
(46) Liu, M., Tanaka, W. N., Zhu, H., Xie, G., Dooley, D. M., and Lei, B. (2008) Direct hemin transfer from IsdA to IsdC in the iron-regulated surface determinant (Isd) heme acquisition system of *Staphylococcus aureus*. *J. Biol. Chem. 283*, 6668−6676.
(47) Gaudin, C. F., Grigg, J. C., Arrieta, A. L., and Murphy, M. E. (2011) Unique Heme-Iron Coordination by the Hemoglobin Receptor IsdB of *Staphylococcus aureus*. *Biochemistry 50*, 5443−5452.
(48) Nygaard, T. K., Blouin, G. C., Liu, M., Fukumura, M., Olson, J. S., Fabian, M., Dooley, D. M., and Lei, B. (2006) The mechanism of direct heme transfer from the streptococcal cell surface protein Shp to HtsA of the HtsABC transporter. *J. Biol. Chem. 281*, 20761−20771.
(49) Bhakta, M. N., and Wilks, A. (2006) The mechanism of heme transfer from the cytoplasmic heme binding protein PhuS to the δ-regioselective heme oxygenase of *Pseudomonas aeruginosa*. *Biochemistry 45*, 11642−11649.
(50) Mattle, D., Zeltina, A., Woo, J. S., Goetz, B. A., and Locher, K. P. (2010) Two stacked heme molecules in the binding pocket of the periplasmic heme-binding protein HmuT from *Yersinia pestis*. *J. Mol. Biol. 404*, 220−231.
(51) Arnesano, F., Banci, L., Barker, P. D., Bertini, I., Rosato, A., Su, X. C., and Viezzoli, M. S. (2002) Solution structure and characterization of the heme chaperone CcmE. *Biochemistry 41*, 13587−13594.
(52) Enggist, E., Thony-Meyer, L., Guntert, P., and Pervushin, K. (2002) NMR structure of the heme chaperone CcmE reveals a novel functional motif. *Structure 10*, 1551−1557.
(53) Daltrop, O., Stevens, J. M., Higham, C. W., and Ferguson, S. J. (2002) The CcmE protein of the c-type cytochrome biogenesis system: Unusual in vitro heme incorporation into apo-CcmE and transfer from holo-CcmE to apocytochrome. *Proc. Natl. Acad. Sci. U.S.A. 99*, 9703−9708.
(54) Stevens, J. M., Daltrop, O., Higham, C. W., and Ferguson, S. J. (2003) Interaction of heme with variants of the heme chaperone CcmE carrying active site mutations and a cleavable N-terminal His tag. *J. Biol. Chem. 278*, 20500−20506.
(55) Ho, W. W., Li, H., Eakanunkul, S., Tong, Y., Wilks, A., Guo, M., and Poulos, T. L. (2007) Holo- and apo-bound structures of bacterial periplasmic heme-binding proteins. *J. Biol. Chem. 282*, 35796−35802.
(56) Grigg, J. C., Vermeiren, C. L., Heinrichs, D. E., and Murphy, M. E. (2007) Haem recognition by a *Staphylococcus aureus* NEAT domain. *Mol. Microbiol. 63*, 139−149.
(57) Sharp, K. H., Schneider, S., Cockayne, A., and Paoli, M. (2007) Crystal structure of the heme-IsdC complex, the central conduit of the

Isd iron/heme uptake system in *Staphylococcus aureus*. *J. Biol. Chem. 282*, 10625−10631.
(58) Ikeda-Saito, M., Hori, H., Andersson, L. A., Prince, R. C., Pickering, I. J., George, G. N., Sanders, C. R., Lutz, R. S., McKelvey, E. J., and Mattera, R. (1992) Coordination structure of the ferric heme iron in engineered distal histidine myoglobin mutants. *J. Biol. Chem. 267*, 22843−22852.
(59) Block, D. R., Lukat-Rodgers, G. S., Rodgers, K. R., Wilks, A., Bhakta, M. N., and Lansky, I. B. (2007) Identification of two heme-binding sites in the cytoplasmic heme-trafficking protein PhuS from *Pseudomonas aeruginosa* and their relevance to function. *Biochemistry 46*, 14391−14402.
(60) Couture, M., Das, T. K., Lee, H. C., Peisach, J., Rousseau, D. L., Wittenberg, B. A., Wittenberg, J. B., and Guertin, M. (1999) *Chlamydomonas* chloroplast ferrous hemoglobin. Heme pocket structure and reactions with ligands. *J. Biol. Chem. 274*, 6898−6910.
(61) Emsley, P., and Cowtan, K. (2004) Coot: Model-building tools for molecular graphics. *Acta Crystallogr. D60*, 2126−2132.